Valeri, Nicola et al. (2014) *microRNA-135b promotes cancer progression acting as a downstream effector of oncogenic pathways in colon cancer.* Cancer Cell, 25 (4). pp. 469-483. ISSN 1535-6108

http://eprints.gla.ac.uk/92699/

Deposited on: 21 May 2014

MicroRNA-135b Promotes Cancer Progression by Acting as a Downstream Effector of Oncogenic Pathways in Colon Cancer

Nicola Valeri,[1,11,*] Chiara Braconi,[1,11] Pierluigi Gasparini,[2] Claudio Murgia,[3] Andrea Lampis,[1,11] Viola Paulus-Hock,[1] Jonathan R. Hart,[4] Lynn Ueno,[4] Sergei I. Grivennikov,[5] Francesca Lovat,[2] Alessio Paone,[2] Luciano Cascione,[2,12] Khlea M. Sumani,[2] Angelo Veronese,[6] Muller Fabbri,[2,13,14] Stefania Carasi,[2] Hansjuerg Alder,[2] Giovanni Lanza,[7] Roberta Gafa',[7] Mary P. Moyer,[8] Rachel A. Ridgway,[3] Julia Cordero,[3] Gerard J. Nuovo,[2] Wendy L. Frankel,[9] Massimo Rugge,[10] Matteo Fassan,[10] Joanna Groden,[2] Peter K. Vogt,[4] Michael Karin,[5] Owen J. Sansom,[3] and Carlo M. Croce[2,*]

[1]Institute of Cancer Sciences, University of Glasgow, Glasgow G61 1BD, UK
[2]Human Cancer Genetics Program, Ohio State University Comprehensive Cancer Center, Columbus, OH 43212, USA
[3]Cancer Research UK Beatson Institute, Glasgow G61 1BD, UK
[4]Department of Molecular & Experimental Medicine, The Scripps Research Institute, La Jolla, CA 92037, USA
[5]Department of Pharmacology, School of Medicine, University of California, San Diego, San Diego, CA 92093, USA
[6]Aging Research Center, G.d'Annunzio University Foundation, Chieti 66100, Italy
[7]Department of Pathology, University of Ferrara, Ferrara 44121, Italy
[8]INCELL Corporation, San Antonio, TX 78249, USA
[9]Department of Pathology, Ohio State University Comprehensive Cancer Center, Columbus, OH 43212, USA
[10]Department of Pathology, University of Padova, Padova 35121, Italy
[11]Present address: The Institute of Cancer Research and The Royal Marsden NHS Trust, Sutton, Surrey SM2 5NG, UK
[12]Present address: Bioinformatics Unit, Lymphoma and Genomics Research Program, Institute of Oncology Research, 6500 Bellinzona, Switzerland
[13]Present address: Department of Pediatrics and Department of Molecular Microbiology & Immunology, Norris Comprehensive Cancer Center, Keck School of Medicine, University of Southern California, Los Angeles, CA 90027, USA
[14]Children's Center for Cancer and Blood Diseases and The Saban Research Institute, Children's Hospital Los Angeles, Los Angeles, CA 90027, USA
*Correspondence: nicola.valeri@icr.ac.uk (N.V.), carlo.croce@osumc.edu (C.M.C.)
http://dx.doi.org/10.1016/j.ccr.2014.03.006

SUMMARY

MicroRNA deregulation is frequent in human colorectal cancers (CRCs), but little is known as to whether it represents a bystander event or actually drives tumor progression in vivo. We show that miR-135b overexpression is triggered in mice and humans by APC loss, PTEN/PI3K pathway deregulation, and SRC overexpression and promotes tumor transformation and progression. We show that miR-135b upregulation is common in sporadic and inflammatory bowel disease-associated human CRCs and correlates with tumor stage and poor clinical outcome. Inhibition of miR-135b in CRC mouse models reduces tumor growth by controlling genes involved in proliferation, invasion, and apoptosis. We identify miR-135b as a key downsteam effector of oncogenic pathways and a potential target for CRC treatment.

INTRODUCTION

Colorectal cancer (CRC) arises through the progressive accumulation of mutations in oncogenes and tumor-suppressor genes (Sjöblom et al., 2006). Targeting driver pathways represents the best option to tailor cancer treatment and improve survival in patients with metastatic cancer (De Roock et al., 2011; Catenacci et al., 2011). Although there has been recent breakthroughs in

Significance

Precision medicine relies on the ability to track cancer-related pathways and target their downstream effectors to minimize drug resistance and increase therapeutic potential. We show that mutations frequently occurring in the colorectal adenoma-carcinoma sequence converge and synergize in promoting the progressive accumulation of miR-135b by conserved mechanisms in mice and humans. In turn, miR-135b acts as one of the driving forces promoting cancer phenotype. We prove that use of anti-miR-135b in CRC mouse models has a significant therapeutic potential. Our results define miR-135b as a key molecule downstream of oncogenic pathways involved in CRC progression, providing the rationale for its use as a robust biomarker and a promising target for therapy.

targeted therapy (e.g., BRAF inhibition), this approach has two main disadvantages: (1) resistance frequently occurs as the result of the activation of collateral pathways circumventing therapeutic blockage (Prahallad et al., 2012), and (2) re-expression of lost tumor-suppressor genes such as *Adenomatous Polyposis Coli* (*APC*) is challenging to translate into drug development.

MicroRNAs (miRs) are a class of small noncoding RNAs involved in cell homeostasis and carcinogenesis (Croce 2009). Several miRs are aberrantly expressed in CRC, and their deregulation is linked to cancer progression and clinical outcome (Valeri et al., 2009). Different oncogenic pathways can converge to affect the same miR and in turn a single miR can control an entire posttranscriptional program affecting dozens of target genes. Because miRs often act as downstream effectors of protein kinases or driver genes mutated in cancer (Croce 2009), targeting miRs may represent a strategy to increase specificity and overcome drug resistance. Preliminary data on the efficacy of miR inhibition are available and prompt the use of anti-miR technology in CRC treatment in vivo (Kasinski and Slack, 2011).

RESULTS

Identification of miRs Dysregulated in CRC Mouse Models

To define miRs deregulated in relation to CRC-specific pathways, we performed a genomewide miR profiling on matched tumor and normal tissues from six mice from two different CRC mouse models: the CDX2P-NLS Cre;Apc$^{+/loxP}$ (CPC;Apc) model harbors a truncating mutation affecting one *APC* allele (Hinoi et al., 2007). In the azoxymethane (AOM)/dextran sulfate sodium (DSS) model (Grivennikov et al., 2009), mice develop CRC as the result of the mutations in several genes including *phosphoinositide 3-kinase* (*Pi3K*), *V-Ki-ras2 Kirsten rat sarcoma viral oncogene homolog* (*K-ras*), *Catenin* (*Cadherine Associated-protein*) *Beta 1* (*Ctnnb1*) and *Proto-oncogene tyrosine-protein kinase Src* (*Src*) pathways (Chen and Huang 2009)

Thirty-five miRs were aberrantly expressed in polyps from the CPC;Apc model with p < 0.001, with seven miRs increased and 14 decreased by greater than 2-fold. In the AOM/DSS model; 57 miRs were aberrantly expressed in tumor compared to normal tissues with p < 0.001; among these, 13 miRs increased and nine decreased by greater than 2-fold (Figure 1A; Tables S1 and S2 available online). We focused on overexpressed miRs because these may be easier to harness as prognostic biomarkers (Croce 2009) or as therapeutic targets compared to downregulated ones (Kasinski and Slack, 2011). MiR-135b was the most overexpressed miR in both models (Figure 1A). RT-PCR and in situ hybridization (ISH) confirmed miR-135b overexpression in tumor tissues (Figures 1B and 1C).

MiR-135b Is Overexpressed in Human CRC

We analyzed 454 sporadic and 31 inflammatory bowel disease (IBD)-associated CRCs to confirm miR-135b upregulation previously reported in smaller CRC cohorts (Necela et al., 2011; Nagel et al., 2008; Gaedcke et al., 2012). A first set including 62 sporadic CRCs was analyzed for miR-135b expression by RT-PCR. MiR-135b expression showed an average 4-fold change in cancer compared to paired normal tissue and correlated with tumor progression as it was increased in the sequence

from stage I to stage IV CRC (Figure 1D, upper). Re-analysis of 392 tumor samples for which tumor stage and miR-135b expression were available from the miR-seq data set of the CRC Cancer Genome Atlas (The Cancer Genome Atlas Network, 2012; Figure 1D) confirmed that miR-135b upregulation follows tumor progression. Paired analysis of matched normal and cancer tissues from the same cohort also showed that miR-135b reads are virtually absent in normal tissues (Table S3), suggesting that miR-135b is a CRC specific deregulated miR; thus, a valuable biomarker and target for therapy.

For IBD-associated CRCs, three different cohorts were analyzed: miR-135b was upregulated by > 7.0-fold in cancer compared to normal tissues in all the different sets. Interestingly, 135b overexpression was found in dysplasia compared to normal tissues, suggesting it might be an early event in colon carcinogenesis (Figure 1D, lower). ISH showed that miR-135b is strongly expressed in the cytoplasm of dysplastic and cancer cells whereas, in line with the TCGA data, little signal is observed in normal mucosa (Figure 1E).

Tumor stage and nodal status were confirmed as prognostic markers in our cohort of sporadic CRC (Figure S1). To test if miR-135b is associated with clinical outcome in CRC, patients were stratified according to the logarithmic ratio between miR-135b expression in cancer and normal tissues: high if log2 miR-135b expression was >2 (above the average miR-135b overexpression observed in Figure 1D), and low if log2 miR-135b expression was ≤2. High miR-135b expression was associated with poor overall survival and relapse-free survival (Figure 1F). A subgroup analysis in patients with stage II CRC identified a trend toward a worse prognosis for patients with high miR-135b. However, the difference was not statistically significant (p = 0.055), likely due to the small sample size (Figure 1F).

MiR-135b Overexpression Is Associated with Mutations in Specific CRC Pathways

Loss of Apc is the initiating mutation in the CPC;Apc model (Hinoi et al., 2007). To confirm that miR-135b overexpression is due to APC loss, we re-induced APC by transfecting a plasmid encoding the *APC* full coding sequence (CDS) in the SW480 human CRC cells, which only contains a mutated *APC* allele leading to a truncated protein (Qian et al., 2008) . Re-expression of wild-type (WT) *APC* caused a 65% reduction in miR-135b expression (p = 0.03), whereas inhibition of *APC* by siRNA resulted in a 5-fold increase (p = 0.01) in miR-135b expression in normal colon epithelial cell lines (Moyer et al., 1996; Figures 2A, 2B, and S2A–S2C) Inactivating mutations in *APC* cause stabilization and nuclear translocation of β-catenin with induction of a complex transcriptional program. To test whether APC loss results in miR-135b overexpression through β-catenin stabilization, we increased β-catenin expression either by transfecting NCM 460 cells with a plasmid encoding the β-catenin transcript or by stabilizing β-catenin with lithium chloride (LiCl) treatment. Both experiments resulted in increased miR-135b expression (3-fold [p = 0.003] and 4.6-fold [p = 0.007], respectively; Figures 2C and S2D). An siRNA screen against the major transcription factors involved in the APC/β-catenin axis was run on two cell lines with high basal β-catenin activity, HCT-116 (β-catenin mutant; Ilyas et al., 1997) and SW480 (*APC* null cells; Qian et al., 2008), revealing that TCF4 and LEF1 silencing causes miR-135b
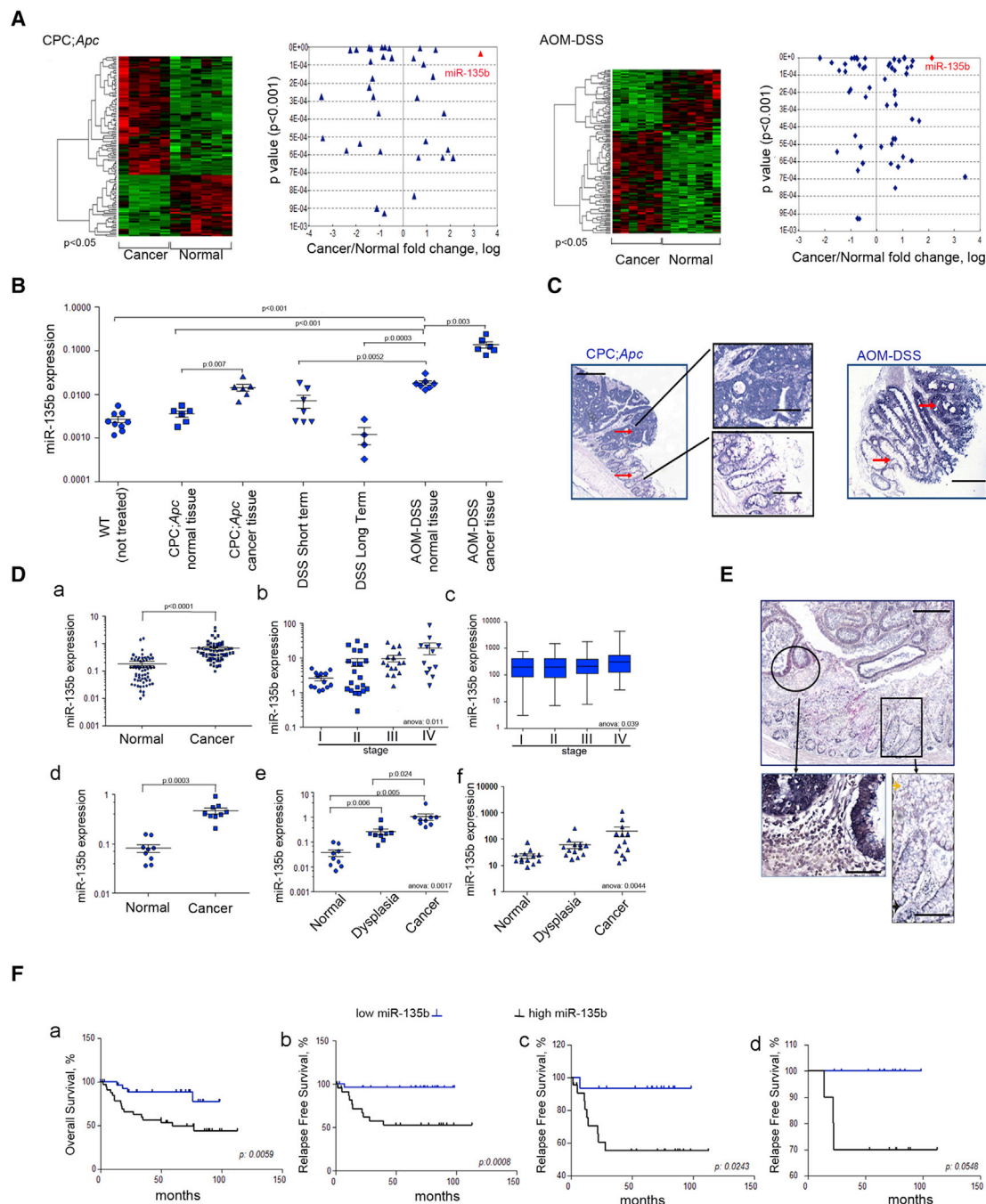
Figure 1. MiR-135b Upregulation in Mouse and Human CRC

(A) Genome-wide miR expression analysis in tumor and normal adjacent colon tissues from CPC;Apc and AOM/DSS treated mice. Selected deregulated miRNAs in cancer relative to normal tissues are plotted against the p value.

(B and C) MiR-135b expression by RT-PCR (B) and ISH (C) in both CRC mouse models. Scale bars, 200 um (100 um in the magnification).

(D) MiR-135b expression was assessed in human tissues. Paired analysis (a) and miR expression according to stage (b) in sporadic CRC (n = 62) are shown. Reads for miR-135b from the TCGA miR-seq data set (n = 392) are shown (c). miR-135b upregulation in three different cohorts of IBD-associated CRC (n = 31): OSU (n = 9; d), University of Ferrara (n = 9; e), and University of Padua (n = 13; f).

(E) ISH for miR-135b in human cancer and normal epithelial cells. Scale bars, 200 um (50 um in the magnification).

(F) Prognosis of sporadic CRC patients according to miR-135b expression: (a) overall survival (OS) in the entire cohort, (b) relapse-free survival (RFS) in stage I-II-III CRC, (c) RFS in stage II-III only CRC and (d) in stage II only CRC. High or low miR-135b expression was defined as low if Log_2-miR-135b-ratio (cancer/normal) ≤ 2 or high if Log_2-miR-135b-ratio > 2.

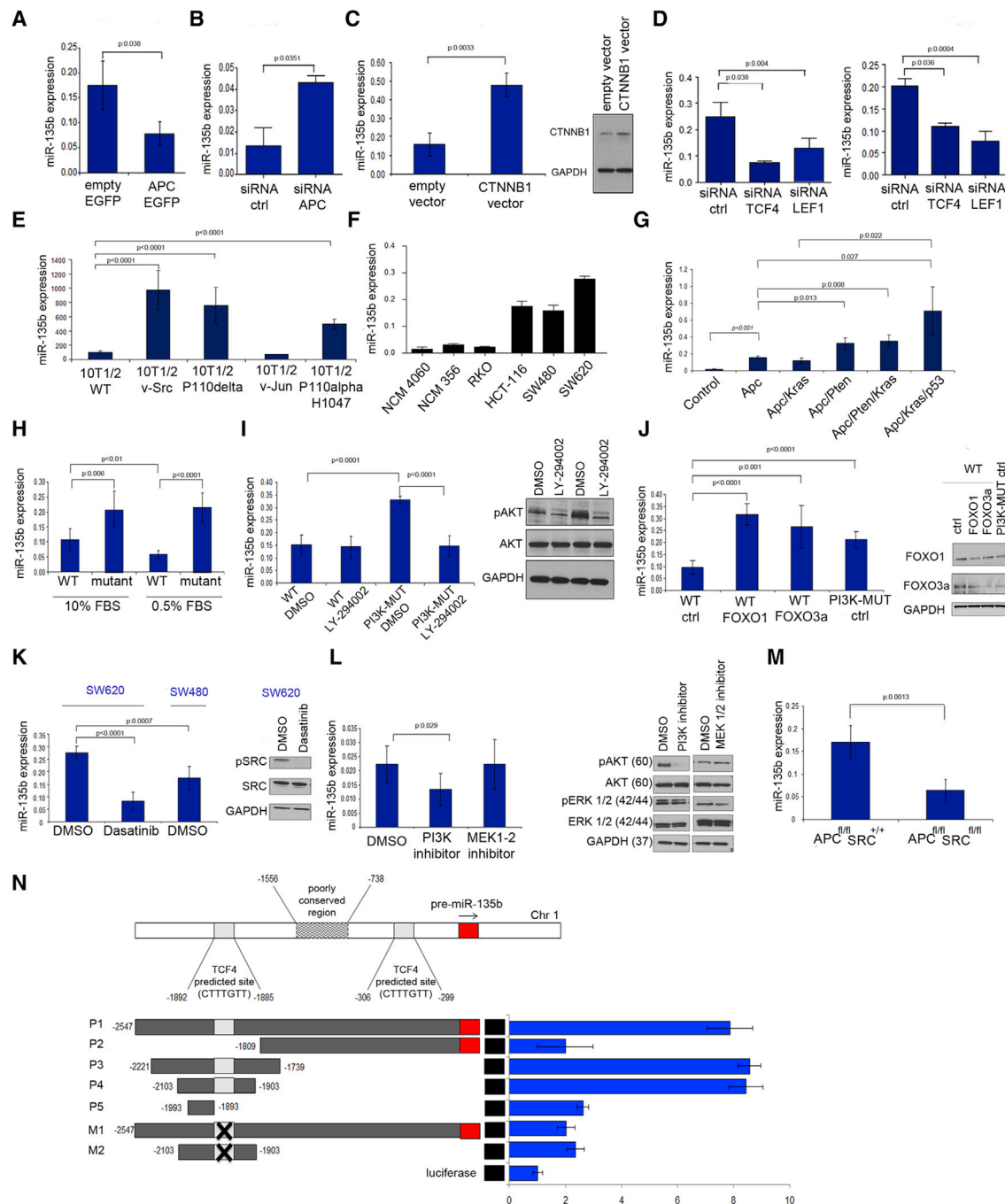See also Tables S1–S3 and Figure S1.

Figure 2. MiR-135b Overexpression Is Associated with Mutations in Specific CRC Pathways

(A) miR-135b expression following transfection with a plasmid encoding the APC CDS in *APC* mutant SW480 cells.

(B) miR-135b expression following APC silencing in normal colon (NCM 460) epithelial cells.

(C) miR-135b expression (left) following overexpression of CTNNB1 (right) in NCM 460 normal epithelial cells.

(D) miR-135b expression following silencing of TCF4 and LEF1 transcription in *APC* mutant SW480 cells (left) or *CTNNB1* mutant HCT-116 cells (right).

(E–G) miR-135b expression in MEFs (E), human normal and CRC cell lines (F), and tumor-derived organoids from GEMMs (G) harboring different rounds of mutations in genes commonly mutated in human CRC.

(H–J) miR-135b expression in *PI3KCA* WT and mutant HCT-116 cells after serum starvation (H), treatment with LY-294002 (I), and transfection with specific siRNAs to FoxO1 and FoxO3A (J).

(K) miR-135b expression in parental SW480 and SW620 CRC cell lines after treatment with dasatinib.

(L) miR-135b expression in Src-MEFs after treatment with PI3K or MEK1/2 inhibitors.

(M) miR-135b expression in tumor derived from *AhCre Apc^fl/fl Src^+/+* and *AhCre Apc^fl/fl Src^fl/fl* mice.

(legend continued on next page)

inhibition (Figures 2D and S2E) . Taken together, these data suggest that miR-135b can be activated by the APC/β-catenin/TCF4-LEF1 pathway.

To study other pathways involved in miR-135b overexpression that may account for the higher expression of miR-135b in AOM/DSS compared to CPC;Apc tumors, we screened miR-135b expression in a series of mouse embryonic fibroblasts (MEFs) engineered to harbor mutations in specific oncogenes and in human CRC cell lines (Figures 2E and 2F). The analysis revealed increased levels of miR-135b (5-fold change; p < 0.001) in cells expressing the H1047R mutant of *PIK3CA*, which encodes the α isoform of the catalytic subunit of PI3K. Expression of the δ isoform of Pi3k and of Src also led to increased levels of miR-135b (7.5 and 9.7, respectively; p < 0.001), whereas viral Jun did not affect the expression of miR-135b (Figure 2E). The effect of PI3K and Src on miR-135b was correlated with their oncogenic potency in 10T1/2 mouse fibroblasts. The cells overexpressing these proteins are morphologically transformed and capable of anchorage-independent growth (Hart et al., 2011). In contrast, the cells expressing v-Jun show fibroblastic morphology, with only a minority of cells producing colonies in agar suspension.

In human CRC cells, miR-135b expression follows the accumulation of mutation in *APC*, *PI3KCA*, and *SRC* (Figure 2F). RKO cells lack mutations in APC/β-catenin, show low basal SRC activity, and harbor an H1047R mutation in *PIK3CA* and are characterized by low miR-135b basal expression. HCT-116 cells are characterized by β-catenin activating mutations, *PI3KCA* mutations, and moderate SRC activity and display increased miR-135b expression. Parental SW480 cells and their metastatic derivative SW620 have the same mutations in *APC*, and no mutations in *PI3KCA*, but have different SRC activity and show high miR-135b expression (da Costa et al., 1999; Samuels et al., 2005; Dehm et al., 2001).

To study the effect of collateral pathways frequently mutated in CRC, we tested miR-135b expression in tumor-derived organoids from CRC genetically engineered mouse models (GEMMs) that underwent different rounds of knock-in or knock-out mutations in *Apc*, *Kras*, *the Phosphatase and Tensin homolog deleted on chromosome TEN* (*Pten*), and *p53* (Figure 2G). In keeping with our initial findings, Apc loss was associated with miR-135b upregulation in comparison to normal controls. Pten is a negative regulator of the PI3K pathway and these genes are mutually lost in breast and CRC cancer (Frattini et al., 2005), thus we decided to use *Pten^{fl/fl}* mice as a model to study PI3K activation in CRC (Marsh et al., 2008). Consistent with our in vitro data, simultaneous loss of Apc and Pten caused further upregulation in miR-135b compared to *Apc^{fl/fl}* organoids. In contrast, *Kras^{G12}*-activating mutations did not affect miR-135b expression. *Apc^{fl/fl}* /*Pten^{fl/fl}* /*Kras^{G12}* triple mutant organoids showed miR-135b deregulation similar to that of the *Apc^{fl/fl}* /*Pten^{fl/fl}* organoids supporting the hypothesis that the PI3K/PTEN pathway exerts a critical role in controlling miR-135b expression. Finally,

loss of p53 caused a 10-fold change in miR-135b compared to *Apc^{fl/fl}* organoids.

To study the role of PI3K in the modulation of miR-135b, we used human CRC cell lines (HCT-116, *H1047R* and DLD-1, and *E545K*) in which either the *PI3KCA* mutant or WT allele was disrupted (Samuels et al., 2005). *PIK3CA* mutations have little effect on cancer phenotype under basal conditions, but they cause reduced cellular dependence on growth factors affecting cell growth and apoptosis in serum starvation. MiR-135b expression is increased in *PI3KCA* mutant compared to WT cells (less than 2-fold change) in basal conditions. Serum starvation forced the *PI3KCA* mutation phenotype, increasing the difference in miR-135b expression (3.7 and 4.3 fold change; p < 0.001 in HCT116 and DLD-1, respectively; Figures 2H and S2F). These experiments suggest that miR-135b is dependent upon PI3K activation. We treated HCT-116 cells with the PI3KCA inhibitor LY294002 after starvation and observed marginal effects on WT cells, but reduction (65%; p < 0.001) of miR-135b in mutant cells (Figure 2I). The transcription factors FoxO1 and FoxO3A promote the PI3K cancer-associated phenotype in these cell lines (Samuels et al., 2005). To investigate whether miR-135b is under the control of the FoxO transcription factors family, we silenced *FoxO1* and *FoxO3A* with siRNA in HCT-116 *PI3KCA* WT cells and observed an increase in miR-135b expression. Silencing FoxO1 and 3A in WT cells increased miR-135b to levels similar to those observed in PI3K mutant cells (Figure 2J). In conclusion, *PI3KCA* mutations may induce miR-135b by phosphorylating and inactivating FoxO1 and FoxO3A or altering FoxO1/3A targets.

SRC is nonmembrane receptor tyrosine kinase (Yeatman 2004) and induces activation of several pathways. MiR-135b was overexpressed in v-Src expressing MEFs compared to WT cells (Figure 2E). Dasatinb, a SRC inhibitor (Serrels et al., 2006), reduced the expression of miR-135b in SW620 CRC cells to levels observed in their parental nonmetastatic counterpart (SW480; Figure 2K). Because SRC can activate a plethora of downstream effectors, we focused only on those previously analyzed in our MEF screening: PI3K and MAPK. Our data suggested that the MAPK pathway is not responsible for miR-135b overexpression because overexpression of v-Jun (Shaulian 2010) showed no effect on miR-135b expression. LY294002 reduced the expression of miR-135b by 40% (p = 0.03) in v-Src expressing MEFs, whereas a MEK1-2 (Yoon et al., 2011) inhibitor did not affect miR-135b expression (Figure 2L). Loss of Src attenuates the intestinal phenotype caused by Apc loss both in flies and mice (J.C. and O.J.S., unpublished data). Interestingly, in our system, loss of Src in AhCRE *Apc^{fl/fl}* mice was associated with a reduction in miR-135b expression (Figure 2M). These observations suggested that, at least in part, SRC induces miR-135b overexpression through the PI3K/AKT/FoxO pathway. However, we cannot rule out the possibility that other SRC effectors contribute to miR-135b overexpression. This hypothesis is supported by the observation that PI3K inhibition only partially

---

(N) Luciferase reporter assay was performed after LiCl treatment using different vectors containing predicted TCF4 binding sites upstream of the pre–miR-135b; −1 position corresponds to the 5′ terminus of the miR-135b hairpin. Putative TCF4 responsive sequences (CTTTGTT)) are indicated in the gray boxes, and the miR-135b sequence is in red. Deletion of the TCF4 binding site is represented by a X.

Human or mouse miR-135b expression was assessed by RT-PCR and normalized to that of RNU48 or SNU234, respectively. Bars represent the mean and SD of three experiments; p values are reported within the figures. See also Figure S2.

reduces miR-135b expression and by the recent observation that STAT3 can induce miR-135b overexpression in large cell lymphomas (Matsuyama et al., 2011).

MiR-135b is located on the negative strand of 1q32.1 and overlaps with exon 1 of the LEM domain-containing 1 (*LEMD1*) gene (Figure S2G). LEMD1 is overexpressed in prostate cancer (Ghafouri-Fard et al., 2010) and anaplastic cell lymphoma (Matsuyama et al., 2011). Gene expression analysis suggests that only a (657 nt) *LEMD1* isoform is expressed in CRC (Yuki et al., 2004).

To test whether miR-135b transcription is depended upon LEMD1 activation, we analyzed the expression of *LEMD1* and miR-135b following inhibition of transcription factors involved in miR-135b expression (Figure S2H). RT-PCR using *LEMD1* primers covering all the different spliced LEMD1 isoforms revealed no change in *LEMD1* expression in relation to TCF4/LEF1 silencing suggesting that miR-135b activation is independent from *LEMD1* in CRC. Because the loss of APC and the activation of the β-catenin/TCF4 pathway seem to be the initiating event in miR-135b deregulation, we subcloned the ∼2.5 kb area up-stream of the 5′ terminus of miR-135b hairpin into the pGL3 reporter vector (PGL3-miR-135b-P1 for the full-length, WT plasmid) and we tested luciferase activity following LiCl stimulation (Figure 2N). Two putative TCF4 binding sites (distal and proximal to the 135b hairpin) were identified in this area (http://genome-euro.ucsc.edu; Figure 2N). Subcloning of the two predicted binding sites and mutagenesis experiments allowed to define the distal binding site as the one involved in miR-135b activation (PGL3-miR-135b-P2/P5 M1-M2; Figure 2N).

We previously showed that FoxO transcription factors exert a negative control on miR-135b activation (Figure 2J). To test whether FoxO binds to miR-135b promoter, we looked for potential FoxO consensus sequences and we identified a conserved area located 300 bp (−289 to 280) upstream of the hairpin precursor. When NCM460 cells were cotransfected with siRNA to FoxO3a or FoxO1 and the PGL3-miR-135b-P1 plasmid, no effect was seen on promoter activation (data not shown), suggesting that FoxOs do not have a direct interaction with miR-135b promoter. Because FoxOs can bind β-catenin preventing the activation of TCF4 (Hoogeboom et al., 2008), we tested whether modulation of Foxo3a would cause any change to promoter activation induced by β-catenin stabilization. Interestingly, silencing of Foxo3a increased miR-135b promoter activation (1.9-fold change; p = 0.004), whereas FoxO overexpression reduced (63% reduction; p = 0.003) the luciferase activity (Figure S2I, blue bars). A TOPFLASH plasmid containing multiple copies of an optimal TCF-binding site and a FOPFLASH plasmid containing multiple copies of a mutant form of a TCF-binding site were used in parallel to confirm TCF4 inhibition by FoxO (Figure S2I, red bars). These data underpin the synergic activity of the PI3K and APC pathways in controlling miR-135b activation, proving that different oncogenic pathways merge on miR-135b activation directly and indirectly.

MiR-135b Affects Apoptosis and Cell Growth

APC/Wnt/β-catenin signaling is pivotal for cell division and is linked to reduced apoptosis (Morin et al., 1996; Groden et al., 1995). To test the contribution of miR-135b on APC/β-catenin-mediated apoptosis, we cotransfected SW480 cells with a plasmid encoding the full *APC* CDS (*APC*-EGFP) or an empty vector (empty EGFP) in combinations with LNA-anti-miR-135b, pre-miR-135b or controls. In line with previous evidence (Morin et al., 1996; Groden et al., 1995), APC re-expression caused apoptosis (Figure 3A). Similarly, the inhibition of miR-135b alone induced apoptosis. The cotransfection of miR-135b and *APC*-EGFP rescued the effect on apoptosis due to the re-induction of APC (Figure 3A). *APC* is a target of miR-135b (Nagel et al., 2008); however, in our experiments the *APC*-EGFP vector contains only the *APC* CDS and not the 3′UTR. These data suggest that re-expression of APC causes apoptosis, at least in part, by downregulating miR-135b.

To test the effects of miR-135b on cell growth, we used HCT-116 *PI3KCA* WT and mutant cells (Samuels et al., 2005). *PI3K* WT cells overexpressing miR-135b showed increased proliferation after 48 hr, and the difference was still statistically significant after 5 days. Similarly, *PI3KCA* mutant cells transfected with anti-miR-135b showed reduced proliferation compared to the LNA-control cells (Figures 3B, S3A, and S3B; Tables S4 and S5). The presence of *PI3KCA* mutations also affected growth in soft agar. Silencing of miR-135b reduced the number of colonies in the *PI3KCA* mutant cells, whereas miR-135b overexpression resulted in increased colony formation (Figures 3C and S3C). Moreover, inhibition of miR-135b in SRC-MEFs inhibited their ability to form colonies in soft agar. Anti-miR-135b or scramble lenti-viral vectors were used to infect SRC-MEFs (Figure 3D). MiR-135b repression caused a 95% reduction (p < 0.001) in the number of colonies in SRC-transformed MEFs (Figures 3E and 3F), supporting the hypothesis that miR-135b is a major driver of SRC-induced transformation.

Targeting miR-135b Affects Tumor Growth In Vivo

Apc loss causes alterations in the crypt-villus architecture promoting classical features of neoplastic transformation such as increased proliferation and loss of differentiation. To investigate the role of miR-135b in Apc loss-mediated transformation in vivo, we designed specific oligonucleotides to target endogenous miR-135b (anti-miR-135b oligonucleotides [miR-135b-AMO] and scrambled-oligonucleotides [Scramble-AMO]). The miR-135b-AMO silencing efficacy was initially tested in vitro and in vivo (Figures S4A and S4B). A custom probe recognizing the miR-135b-AMO oligonucleotides was used for ISH and revealed a strong signal in colon epithelium, suggesting that the miR-135b-AMO was taken up and retained in mice intestine for at least 48 hr following injection (Figure S4B). Off-target effects of miR-135b-AMO on other miRs were excluded (Figure S4C).

To study the contribution of miR-135b to the phenotype induced by APC loss, we triggered rapid *Apc* inactivation by the administration of β-napthoflavone to *AhCre+Apc^fl/fl* mice as previously described (Sansom et al., 2004). MiR-135b-AMO and Scrambled-AMO were given intraperitoneally at a dose of 50 mg/kg on days 2 and 4 and mice were euthanized on day 4 (Figure 4A). *Apc* inactivation was associated with β-catenin activation and nuclear localization in both treatment groups (Figure S4D). Apc loss caused a 10-fold increase in miR-135b expression in *Cre+Apc^fl/fl* compared to *Cre+Apc^+/+* controls (WT hereafter) definitively showing that mir135b is directly activated following Apc loss. MiR-135b-AMO caused a marked reduction in miR-135b expression (70%; p < 0.001) in the
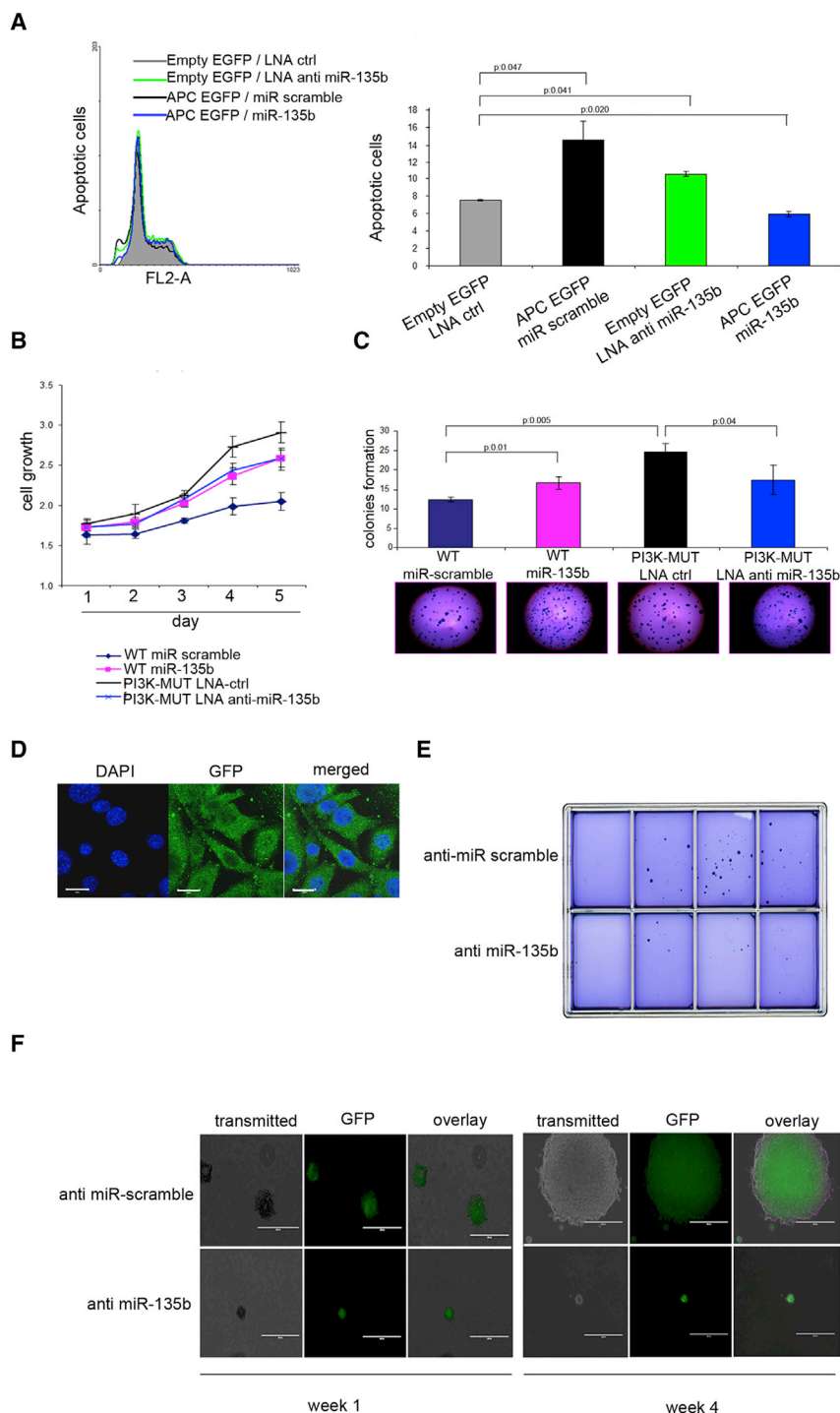
Figure 3. MiR-135b Mediates the Cancer Phenotype Induced by *APC* and *PI3KCA* Mutations

(A) *APC* mutant SW480 cells were transfected with pre-miR-135b, LNA anti-miR-135b, or controls in combination with a plasmid encoding the *APC* CDS or an empty vector. Apoptotic cells were measured by flow cytometer (left) and quantitated (right).

(B) Isogenic *PI3KCA* WT and mutant HCT-116 cells were transfected with pre-miR-135b, LNA anti-miR-135b, or relative controls. Cell viability was measured at selected time points.

(C) Isogenic *PI3KCA* mutant and WT HCT-116 cells overexpressing miR-135b or anti-miR-135b were plated in soft agar and grown in low fetal bovine serum conditions. Colonies greater than 2 mm in size were counted and quantitated. Representative images are shown.

(D–F) v-SRC transformed MEFs were infected with lentiviruses encoding an anti-miR-135b or a scramble hairpin. Cells were selected with puromycin and checked for viral integration using GFP (scale bars, 20 um; D). Cells were grown in soft agar and colonies were counted after 4 weeks. On the far left of the plate, no cells were seeded as negative control (E). GFP was used to monitor viral integration during for the entire duration of the experiment (F). Scale bars, 200 um (week 1) and 400 um (week 4). Bars represent the mean and SD of three experiments; p values are reported within the figures. See also Tables S4 and S5 and Figure S3.

4B and 4C). In the *Cre⁺Apcᶠˡ/ᶠˡ* 135b-AMO, a normal morphology was retained, cellularity and number of mitosis (54.8 ± 3; p 0.02 and 1.6 ± 0.7, respectively) were importantly reduced compared to scrambled-AMO mice (Figures 4B and 4C). To define changes in proliferation, mice from all the three groups (n = 3) were injected with BrdU and killed 2 hr later on day 4. Scoring of the proportion of cells in S phase revealed a 43% increase in proliferation in the scrambled-AMO mice compared to the WT mice (BrDU-positive cells 40.5 vs. 28.4; p = 0.01). 135b-AMO mice showed decreased proliferation compared to scrambled-AMO (mitotic index: 27.1; p = 0.02) and no difference compared to the WT mice (Figure 4B, right) with a clear cleavage plain between the expected mid crypt proliferation region and the upper compartment (Figure 4C).

miR-135b-AMO-treated mice (n = 6 [135b-AMO mice hereafter]) compared to scrambled-AMO-treated mice (n = 6 [scrambled-AMO mice hereafter]; Figure S4E). In the scrambled-AMO, loss of the crypt structures and occupation of the crypt-villus axis by atypical cells was observed; indeed, cellularity was doubled compared to that of WT mice (89.8 ± 6 cells per crypt VS 41.6 ± 2.3 cells per crypt; p = 0.0001) and the number of mitotic figures per crypt was increased (average 3.16 vs. 1.35; p = 0.03; Figures

Because the AOM/DSS better resembles the high level of genetic instability observed in human CRC (The Cancer Genome Atlas Network, 2012) compared to the CPC;Apc model, we tested this model to study the therapeutic potential of 135b-AMO in vivo. Colorectal carcinogenesis was induced using the AOM/DSS protocol and 135b-AMO or scrambled-AMO were administered simultaneously twice a week for the entire duration of the treatment (Figure 5A). After 100 days, the mice were
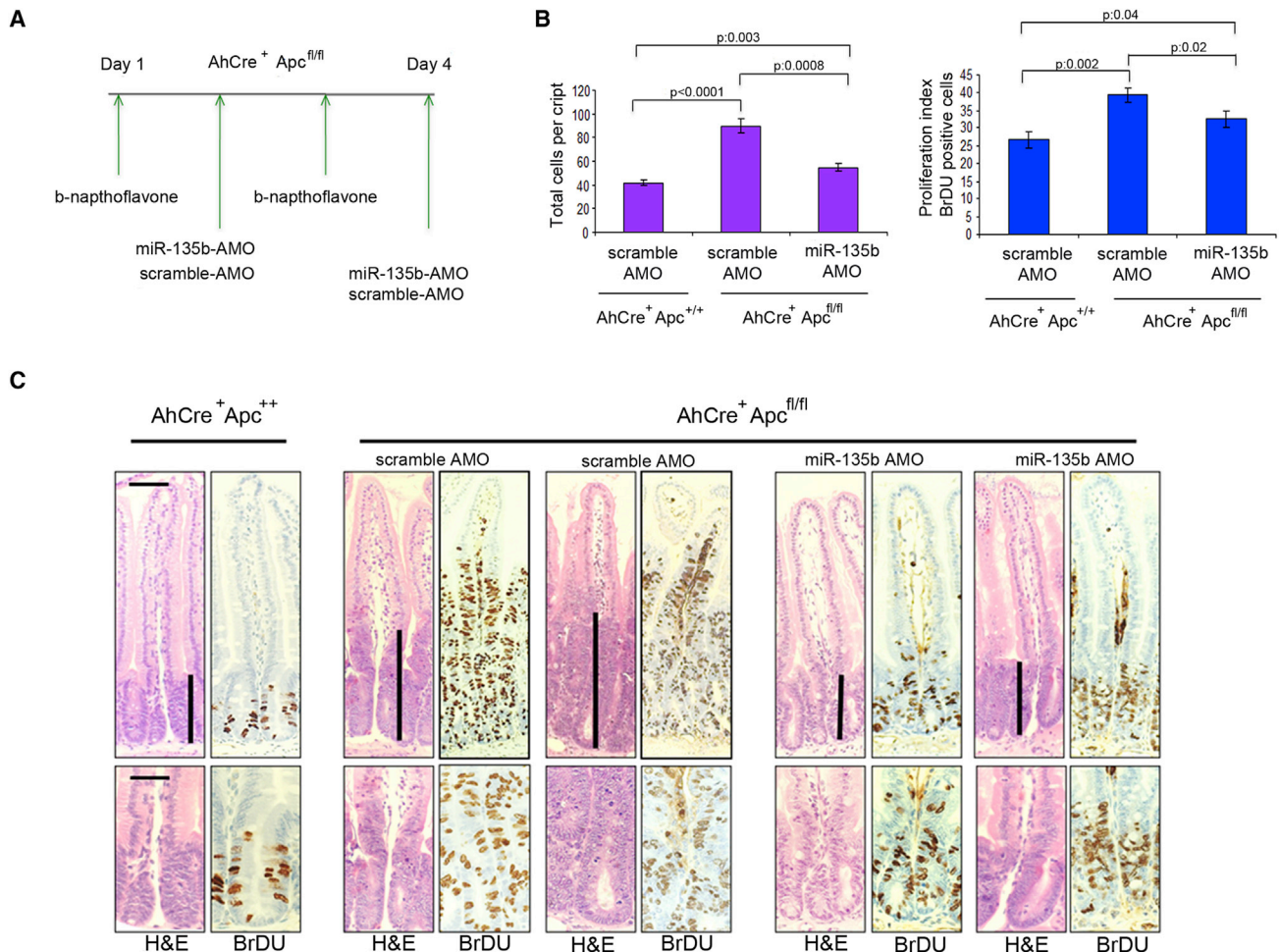
Figure 4. miR-135b Inhibition Rescues Apc-Induced Phenotype In Vivo

(A) Conditional *Apc* deletion induced by b-napthoflavone injection in *AhCre+Apc+/+* mice on days 1 and 3. miR-135b-AMO or scrambled-AMO were injected on days 2 and 4. Mice (n = 6 for each group) were euthanized on day 4.

(B) Graphs show total cells per crypt (left) and proliferation index (ratio between BrDU-positive cells and total cells per crypt; right) in *AhCre+Apc+/+* and *AhCre+Apcfl/fl* mice treated with scramble-AMO or anti-135b-AMO. BrDU was injected in three mice per group 2 hr prior to euthanization. Error bars represent SD; p values are shown within the graphs. Magnification bars, 100 um (top), 50 um (bottom).

(C) Hematoxylin and eosin (H&E) and BrDU-stained sections for AhCre+Apc+/+ and AhCre+Apcfl/fl mice treated with scramble-AMO or anti-135b-AMO. Bars show size of the crypts. Magnification bars, 100 um (top), 50 um (bottom).

See also Figure S4.

euthanized and tumors were analyzed (Figures 5B and 5C). None of the mice showed signs of toxicity related to AMO treatment or had to be euthanized before the end of the study due to toxicity.

MiR-135b-AMO reduced the median number and the size of tumors (Figures 5B–5D). No differences were observed between the scrambled-AMO and the control group. Microscopy showed that MiR-135b-AMO tumors were well differentiated with an acinar pattern, whereas tumors in the scrambled-AMO group showed poor differentiation and an adenomatous pattern (Figure 5C). Effective miR-135b downregulation in 135b-AMO treated mice was confirmed by RT-PCR and ISH (Figures S5A and S5B). Proliferation was remarkably reduced in tumors from miR135b-AMO compared to scrambled-AMO (Ki-67 positive cells 60% vs. 35% p < 0.01; Figure 5E). Apoptosis was analyzed by an immunofluorescence-based

TUNEL assay. The percentage of apoptotic cells and the intensity of the signal were increased in the anti-miR-135b tumors in comparison to the scrambled-AMO tumors (Figure 5F). No significant differences were observed in other organs (Figure S5C).

To dissect the contribution of miR-135b overexpression to each single pathway, we infected CRC GEMM-derived organoids with lentiviruses silencing miR-135b or controls; we xenotransplanted the tumors in nude mice and monitored tumor growth (Figure 6A). Given that *Apcfl/fl/Ptenfl/fl* and *Apcfl/fl/KrasG12/+/P53R172H/fl*-derived organoids were the two models that showed progressive deregulation of miR-135b compared to *Apcfl/fl* organoids, these were used for the experiments. *Apcfl/fl/KrasG12/+* organoids did not show any significant difference in miR-135b expression compared with *Apcfl/fl* and were
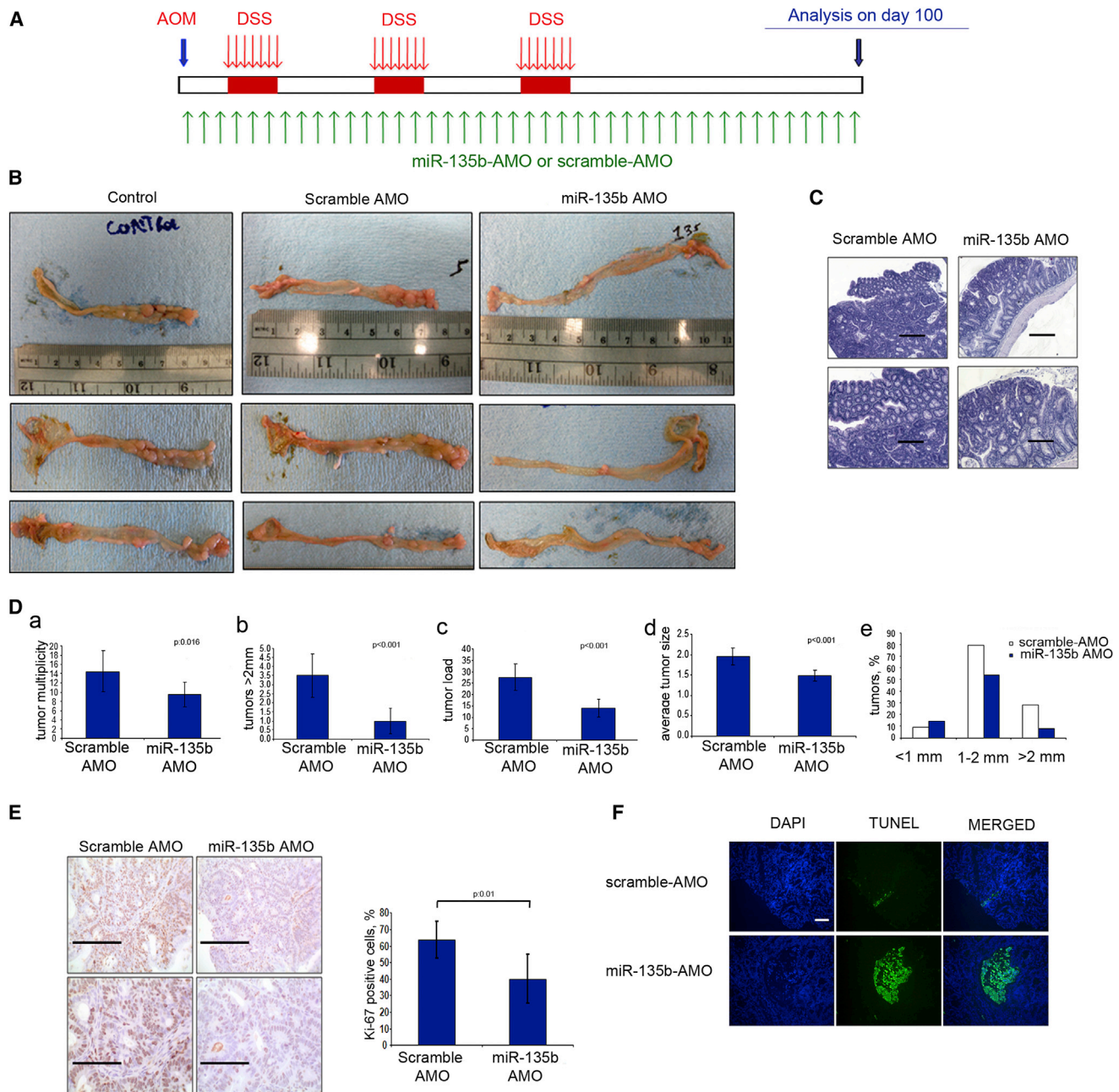
Figure 5. Anti-miR-135b Exerts an Antitumor Effect In Vivo in the AOM/DSS Model

(A–C) Overview of the study (A): AOM was given once, followed by periodic administration of DSS in water. MiR-135b-AMO or scrambled-AMO were given twice a week for 100 days. Mice were treated with miR-135b-AMO (n = 8), scrambled-AMO (n = 8), or left untreated (n = 8). Following euthanization, macroscopic (B) and microscopic (C) analysis of the tumors was performed. Scale bars, 200 um (top), 100 um (bottom).

(D) Statistical analysis of tumor number (multiplicity, a), tumor number for tumors >2 mm (b), tumor volume (load, c), average size (d), and tumor size distribution in the two groups (e).

(E and F) Cancer tissues from mice treated with miR-135b-AMO or scrambled-AMO were analyzed. (E) Ki-67 expression was assessed with immunohisto-chemistry (a) and quantitated (b; scale bars, 200 um [top], 100 um [bottom]). (F) Apoptosis was assessed by immunofluorescence (scale bar, 200 um).

See also Figure S5.

not included. *Apc*^{fl/fl} cells grow slowly in xenografts and for this reason were not included in the study.

For each genotype, organoids were infected with lentiviral vectors inhibiting miR-135b (anti-135b) or controls (anti-miR-scramble; Figure 6B). Mir-135b downregulation was checked by RT-PCR following infection and puromycin selection (Figure 6C). Xenotransplanted tumors (50 organoids for each mouse, six mice per group) were measured twice a week for 2 months or
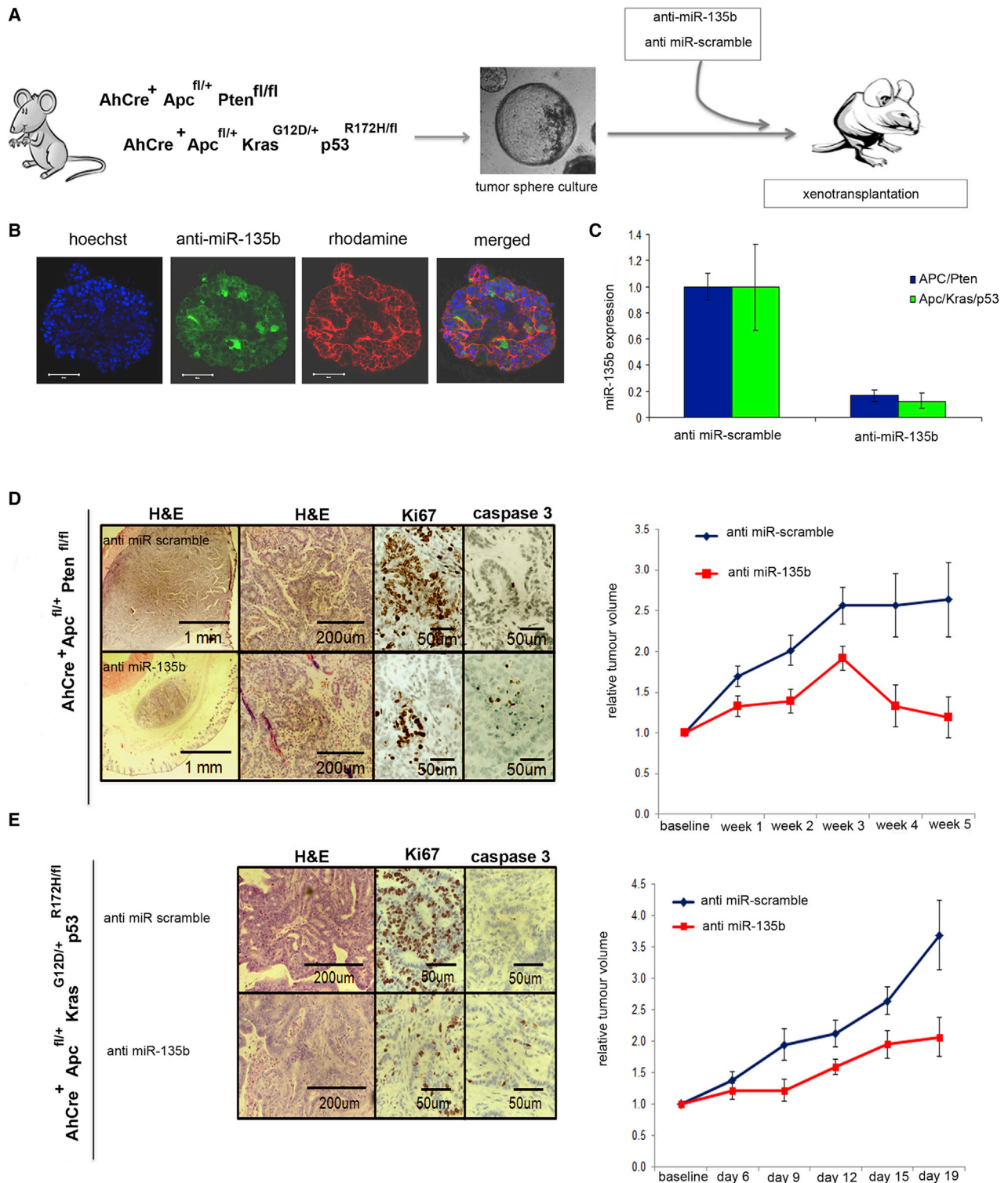
Figure 6. miR-135b Inhibition Causes Tumor Inhibition in Organoids Derived from CRC GEMMs

(A and B) Tumor-derived organoids from $Apc^{fl/fl}/Pten^{fl/fl}$ and $Apc^{fl/fl}/Kras^{G12/+}/P53^{R172H/fl}$ (A) infected with lentiviruses encoding anti-miR-135b or scramble hairpins (B) were xenotransplanted in nude mice. Tumors were measured twice a week for 8 weeks or until ulceration.

(C) miR-135b expression was assessed by RT-PCR in tumor-derived organoids after infection. Bars represent the mean and SD of three experiments; p < 0.01.

(D) Microscopic analysis (left) and tumor growth (right) in $Apc^{fl/fl}/Pten^{fl/fl}$ organoids.

(E) Microscopic analysis (left) and tumor growth (right) in $Apc^{fl/fl}/Kras^{G12/+}/P53^{R172H/fl}$ organoids.

Results are expressed as the mean percentage of change in tumor volume for each group of mice, ± SEM. See also Figure S6 and Tables S6 and S7.

until tumor ulceration. At the end of the study, tumors were harvested and analyzed for proliferation and apoptosis. Lentiviral integration and miR-135b downregulation were controlled by GFP staining and RT-PCR, respectively (Figure S5).

In the $Apc^{fl/fl}/Pten^{fl/fl}$, we observed striking differences in tumor growth (Figure 6D; Table S6). Six weeks following transplantation, three of six tumors regressed to the point that they could not be detected macroscopically and the other three showed a cessation of growth. Immunohistochemical analysis showed that proliferation was almost entirely abolished in the miR-135b group compared to controls (Figure 6D).

$Apc^{fl/fl}/Kras^{G12/+}/P53^{R172H/fl}$ xenografts infected with anti-miR-scramble grew rapidly, and four of six tumors ulcerated after 3 weeks (Figure 6E; Table S7). In contrast, anti-135b tumors only doubled in 3 weeks and no ulceration was observed until week 8. Tumor growth was inhibited in the anti-135b group and this was supported by the observation that proliferation was inhibited in the lenti-135b group compared to controls (Figure 6E).

MiR-135b Targets Tumor-Suppressor Genes

To find potential target genes affected by miR-135b overexpression, we performed a gene expression analysis in normal epithelial colon cells overexpressing miR-135b (Figure 7A). The analysis of a cancer-associated gene panel revealed that 35 genes were dysregulated by miR-135b overexpression (Table S8). A matched analysis of miR-135b downregulated genes and target prediction algorithms (Lewis et al., 2003; Rehmsmeier et al., 2004) showed that several genes were potentially controlled by miR-135b: transforming growth factor β receptor 2 (TGFβR2), death-associated protein kinase 1 (DAPK1), and APC. Data from the array analysis were confirmed by RT-PCR in the same cell line and in a second normal epithelial cell line (NCM 356; Figures 7B and S7A). We identified predicted binding sites for miR-135b in each of these genes (Lewis et al., 2003; Rehmsmeier et al., 2004; Figure 7C). Luciferase experiments confirmed the specificity of the miR-135b-target interaction (Figure 7D).

DAPK1 is frequently downregulated in CRC, and promoter methylation does not seem to be the main mechanism by which this occurs (Xu et al., 2004; Borinstein et al., 2010). Western blot analysis proved that miR-135b can affect DAPK1 protein expression (Figure 7E). Analysis of DAPK1 expression in human IBD-associated CRC confirmed the downregulation of this gene in cancer and dysplasia compared to normal tissues (Figure 7F). Correlation analysis between miR-135b expression and DAPK1 mRNA showed an inverse correlation (r = −0.4, p = 0.036).

TGFβR2 downregulation is common in CRC (Biswas et al., 2004; Guda et al., 2001) and in vitro evidence suggests that dynamic changes in TGFβR2 expression can have an effect on p21-mediated/TGF-β-induced apoptosis (Rojas et al., 2009). Stimulation of cells with TGF-β (10 nM) induced p21 activation in scrambled transfected cells whereas miR-135b overexpression or TGFβR2 silencing caused reduced p21 activation and reduced apoptosis (Figures 7G and 7H). These data suggest that the miR-135b effect on apoptosis is partially mediated by TGFβR2 downregulation. Analysis of TGFβR2 expression in IBD-associated CRC showed TGFβR2 downregulation in cancer compared to normal and dysplastic tissues (Figure 7I). Correlation analysis between miR-135b expression and TGFβR2 mRNA showed an inverse correlation (r = −0.46, p = 0.015).

Our gene expression analysis revealed that miR-135b upregulation induces interleukin 8 (IL8) overexpression (Table S8; Figures 7J and S7B). IL-8 is an important cytokine involved in proliferation, invasion, migration, and neo-angiogenesis (Waugh and Wilson 2008). IL-8 is frequently involved in hypoxia response; thus, we looked at whether miR-135b could have an effect on IL-8 through HIF1α transcriptional regulation. No changes in HIF1α mRNA were observed following miR-135b overexpression (fold change 1.01; p = 0.77; Table S8), suggesting that IL8 overexpression was independent from HIF1α transcriptional regulation. Because our experiments were performed in condition of normoxia, we looked for a nontranscriptional regulator of HIF1α and searched for potential miR-135b binding sites in HIF1α regulators. FIH is an asparagine hydroxylase that prevents HIF1α activation in normoxia (Mahon et al., 2001). Interestingly FIH harbors a miR-135b binding site (Figure 7K). We proved FIH as a target of miR-135b (Figures 7K–7M and S7C). To support a role of miR-135b in FIH regulation in vivo, we measured FIH mRNA expression in human IBD-associated CRC and found the gene was downregulated in cancer compared to normal and dysplastic tissues (Figure S7D). Correlation analysis between miR-135b expression and FIH mRNA showed an inverse correlation (r = −0.42; p = 0.02). To confirm that miR-135b controls IL-8 production through FIH/HIF1α, we measured IL8 and VEGFA expression after miR-135b manipulation (Figures 7N and S7E). MiR-135b promoted IL-8 and VEGFA overexpression and a similar effect was caused by FIH silencing or by hypoxia. Interestingly HIF1α siRNAs were able to rescue the effect on IL-8 and VEGFA by miR-135b. These observations suggested that miR-135b was acting on both cytokines through a FIH/HIF1α axis (Figure 7N). To test if the increase in IL-8 induced by miR-135b was relevant in promoting a functional effect on neo-angiogenesis, the supernatant from miR-135b overexpressing cells was used for a neo-angiogenesis assay. HUVEC grown with media from miR-135b transfected cells showed a 3-fold change increase in their ability to form tubes compared to those cultured with media from scrambled transfected cells (Figure 7O).

DISCUSSION

Using in vitro and in vivo models, we define the genetic events driving miR-135b deregulation in CRC. Our observations explain why miR-135b upregulation is consistently observed in human and mouse CRC (Nagel et al., 2008; Gaedcke et al., 2012), making this miR a robust and reproducible biomarker. Our findings complement those of a recent report that identifies miR-135b as one of the most upregulated miRs in $Apc^{min/+}$ mice (Necela et al., 2011), suggesting that miR-135b deregulation is independent of the specific Apc mutation or site of inactivation. Data from mouse tumors and human dysplastic tissues suggest that miR-135b upregulation is an early event in tumor transformation as supported by the observation that miR-135b is directly linked to rapid Apc loss in the $AhCreApc^{fl/fl}$ model and inhibition of miR-135b rescues the phenotype induced by Apc loss in a way that resembles c-Myc deletion in mice intestines (Sansom et al., 2007). According to our siRNA experiments, miR-135b regulation seemed to be independent from c-Myc activation; thus, these two factors may control collateral transcriptional programs
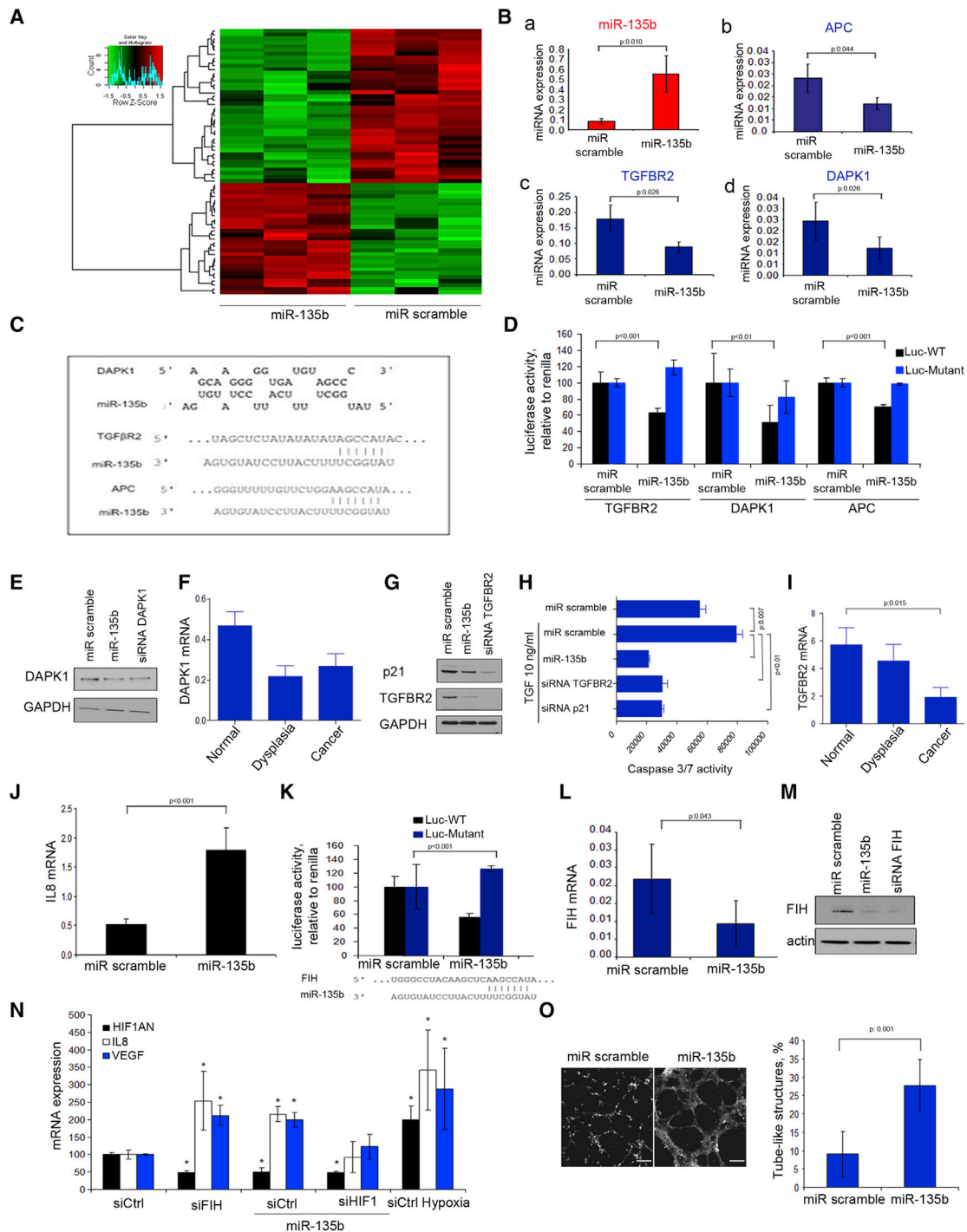
Figure 7. MiR-135b Controls Tumor-Suppressor Genes

(A) Analysis of a cancer gene-associated panel in 460NCM cell transfected with pre-miR-135b or scrambled probes.

(B) *APC (b)*, *TGFβR2* (c), and *DAPK1* (d) mRNA expression analyzed by RT-PCR following miR-135b overexpression (a).

(C) In silico target prediction for miR-135b binding sites in *APC*, *TGFβR2*, and *DAPK1* 3′UTRs.

(D) Luciferase experiments for *TGFβR2*, *DAPK1*, and *APC* in NCM460 cells transfected with target-gene-Luc-WT or target-gene-Luc mutant, pre-miR-135b, or scrambled miR.

(E) DAPK1 protein expression by WB following transfection with pre-miR-135b and specific siRNA.

(F) *DAPK1* mRNA expression in dysplasia and cancer compared to normal adjacent tissues in IBD-associated CRC.

(G and H) TGFβR2 and p21 protein expression assessed following miR-135b overexpression and TGF-β stimulation (G). Apoptosis measured by caspase 3/7 assay following TGF-β stimulation (H).
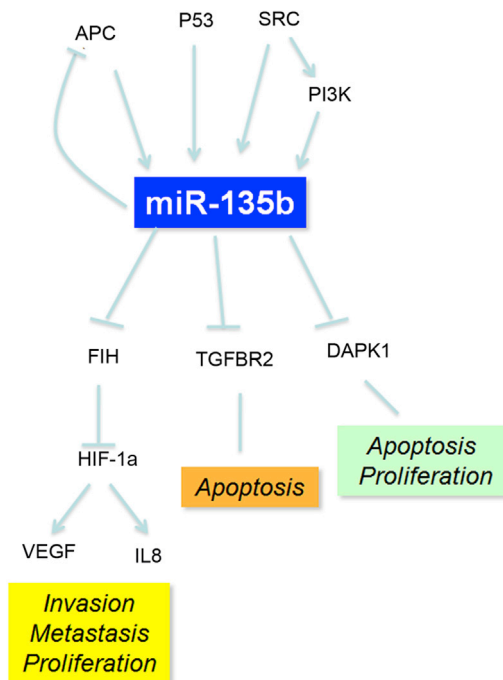
(legend continued on next page)

Figure 8. MiR-135b Is a Key Oncogenic Hub Mediating the Cancer Phenotype Downstream of Genes Frequently Mutated in CRC
Schematic representation of genetic aberrations promoting miR-135b overexpression and miR-135b downstream targets.

of several pathways on miR-135b transcriptional regulation as suggested by the analysis of miR-135b promoter activation. Because miR-135b overexpression follows the kinetics of mutations in CRC, it may represent a good biomarker of tumor progression.

Crosstalk among different pathways is frequently observed in colon carcinogenesis and may affect miR-135b expression at different stages of disease and in different epithelial compartments (progenitor versus mature cells). In IBD-associated cancers, for example, PI3K feeds positively on the Wnt pathway, causing β-catenin phosphorylation and nuclear β-catenin accumulation in progenitor epithelial cells (Lee et al., 2010). Thus, PI3K mutations might have a feed-forward effect on miR-135b expression in this setting. As previously shown (Nagel et al., 2008), miR-135b in turn can control *APC* expression. The presence of this complex feedback loop (Figure 8) might explain several in vivo observations. First, several pathways converging on the same miR explain why no correlation has been previously found between *APC* mutations and miR-135b expression (Nagel et al., 2008). Second, the feedback loop might be responsible for the fine-tuning of miR-135b and the generation of a threshold effect on its target *APC*. IBD-associated CRCs are characterized by rare mutations in the Wnt pathway (Aust et al., 2002) and miR-135b overexpression. According to these observations, we would expect most IBD cancers to show low APC expression and nuclear β-catenin accumulation. On the contrary, only 30%–50% of IBD-invasive tumors show nuclear β-catenin with little or no accumulation in low- or high-grade dysplasia (Leedham et al., 2009). Several reports (Valeri et al., 2010; Mukherji et al., 2011) suggest the presence of a threshold effect in miR function. We speculate that miR-135b deregulation might be responsible for APC loss and β-catenin stabilization only in the fraction of IBD tumors for which miR-135b expression has reached a defined threshold.

MiR-based therapeutics represent a promising approach to tailor cancer therapy; however, off-target effects may represent a major issue for those microRNAs involved in physiological conditions such as miR-21 (Han et al., 2011). Contrary to other miRs, miR-135b basal expression is very low in normal epithelium and other organs as supported by the TCGA analysis. The low miR-135b expression in normal epithelium may be explained either by the observation that, as observed for other Wnt targets (i.e., Lgr5 or Ascl2), a limited number of normal epithelial cells are under Wnt control in physiological conditions or by the observation that transcription factors such as FoxOs or USF1 may act as brakes on miR-135b transcription in physiological conditions. For these reasons, silencing miR-135b in CRC may represent a promising targeted therapy characterized by high specificity and limited toxicity.

orchestrating the tumor initiation process. Indeed, even though proliferation was completely inhibited by miR-135b, some differences between the WT and the 135b-AMO mice were still observed in term of total number of cells per crypt, suggesting that other pathways independent from miR-135b regulation may still be active upon miR-135b inhibition. A second potential explanation to this observation may be technical in nature and related to the ability to silence miR-135b completely by oligonucleotides as compared to complete knockdown caused by Myc deletion in Sansom's model.

Compared to other downstream effectors of the Apc/β-catenin pathway, such as cyclin D1, that are mostly involved in tumor initiation rather than progression (Sansom et al., 2005), miR-135b seems to retain its malignant potential in more advanced carcinogenesis as suggested by the observation that tumor growth was deeply affected by miR-135b silencing in organoids harboring *Apc*, *Pten*, and *p53* mutations. Our data suggest that the progressive upregulation of miR-135b in more advanced tumors may be caused by the convergence

(I) *TGFβR2* mRNA expression in dysplasia and cancer compared to normal adjacent tissues in IBD-associated CRC.
(J) *IL8* mRNA expression following miR-135b overexpression in NCM460 cells.
(K) Luciferase assay in NCM460 transfected with FIH-Luc-WT or FIH-gene-Luc mutant vectors, pre-miR-135b, or scrambled miR. MiR-135b seed region in *FIH* 3′UTR is shown.
(L and M) *FIH* mRNA (L) and protein (M) expression following miR-135b overexpression in 460NCM cells.
(N) *FIH*, *IL8*, and *VEGFA* mRNA following siRNA transfection. *$p < 0.05$.
(O) Tube formation in HUVEC cells cultured with media from scrambled or miR-135b transfected cells: representative picture (left) and normalization (right) are shown.
Bars represent the mean and SD of three experiments; p values are reported within the figures. See also Table S8 and Figure S7.

EXPERIMENTAL PROCEDURES

MiR and mRNA Expression Analysis

MiR expression profiling and mRNA expression of cancer-associated genes were analyzed with nCounter from NanoString Technologies, using the nCounter Mouse miRNA Expression assay kit and the nCounter Human Cancer reference kit, respectively. The NanoString nCounter gene expression system quantitates abundances of miRNAs and mRNA.

Technical normalization is performed using the synthetic positive controls to adjust the counts for each miRNA target in that assay. Then biological normalization is performed to correct for differences in sample abundances. Each sample is normalized to the geometric mean of the top 50 most highly expressed miRs. Student's t test is used on normalized counts to calculate statistical significances of pairwise comparisons. All of the calculations are performed in R statistical computing and graphics environment (http://www.r-project.org).

Animal Experiments and Tumor Induction

RNAs from CpC/Apc (matched tumor and normal), AOM/DSS (matched cancer and normal), wild-type (untreated normal epithelium), and short-term (3–5 days) DSS-treated mice (inflamed epithelium) for the initial miR expression screening were provided by Prof. Michael Karin (University of California at San Diego). RNA from the intestinal epithelium of long-term (three cycles [1 week each] over a 78 day period) DSS-treated mice was collected at Ohio State University (OSU). All mice were C75BL/6 strain mice. For in vivo silencing experiments, C57BL/6 mice were obtained from The Jackson Laboratory. All mice were maintained in filter-topped cages on autoclaved food and water at OSU according to National Institutes of Health guidelines, and all experiments were performed in accordance with OSU and NIH guidelines and regulations. CAC was induced as previously described (Grivennikov et al., 2009). All experiments were approved by the Ethical Review Process of The University of Glasgow. Experiments were carried out in compliance with UK Home Office Animal (Scientific Procedures) Act 1986 and the EU Directive 2010.

Human Tissue Collection

Fresh-frozen and paraffin-embedded tissues from sporadic and IBD-related CRC were collected following informed consent and approval of the ethical committees at (1) Istituto Scientifico Romagnolo per lo Studio e la Cura dei Tumori; (2) Ohio State University Pathology Archive; (3) Department of Pathology, University of Ferrara; and (4) Department of Pathology, University of Padova.

ACCESSION NUMBERS

The Gene Expression Omnibus (GEO) accession numbers for miRNA and mRNA expression data are GSE54177 (mouse tissue) and GSE54163 (human cell lines).

SUPPLEMENTAL INFORMATION

Supplemental Information includes Supplemental Experimental Procedures, seven figures, and eight tables and can be found with this article online at http://dx.doi.org/10.1016/j.ccr.2014.03.006.

AUTHOR CONTRIBUTIONS

N.V., C.B., P.G., C.M., A.L., V.P.-H., J.R.H., L.U., S.I.G., F.L., A.P., K.M.S., A.V., M.F., S.C., R.A.R., and J.C. performed experiments; L.C. performed bioinformatics analysis; H.A. provided support and analyzed data for nCounter analysis; G.L., R.G., W.L.F., M.R., and M.F. provided human samples and provided support for immunohistochemistry; G.J.N. analyzed data for in situ hybridization; M.P.M. provided support with the human normal epithelial cell lines; N.V., C.B., J.G., P.K.V., M.K., O.J.S., and C.M.C. analyzed data and provided funding for the study; and N.V., C.B., and C.M.C. wrote the paper.

ACKNOWLEDGMENTS

REFERENCES

Aust, D.E., Terdiman, J.P., Willenbucher, R.F., Chang, C.G., Molinaro-Clark, A., Baretton, G.B., Loehrs, U., and Waldman, F.M. (2002). The APC/beta-catenin pathway in ulcerative colitis-related colorectal carcinomas: a mutational analysis. Cancer *94*, 1421–1427.

Biswas, S., Chytil, A., Washington, K., Romero-Gallo, J., Gorska, A.E., Wirth, P.S., Gautam, S., Moses, H.L., and Grady, W.M. (2004). Transforming growth factor beta receptor type II inactivation promotes the establishment and progression of colon cancer. Cancer Res. *64*, 4687–4692.

Borinstein, S.C., Conerly, M., Dzieciatkowski, S., Biswas, S., Washington, M.K., Trobridge, P., Henikoff, S., and Grady, W.M. (2010). Aberrant DNA methylation occurs in colon neoplasms arising in the azoxymethane colon cancer model. Mol. Carcinog. *49*, 94–103.

Cancer Genome Atlas Network (2012). Comprehensive molecular characterization of human colon and rectal cancer. Nature *487*, 330–337.

Catenacci, D.V., Kozloff, M., Kindler, H.L., and Polite, B. (2011). Personalized colon cancer care in 2010. Semin. Oncol. *38*, 284–308.

Chen, J., and Huang, X.F. (2009). The signal pathways in azoxymethane-induced colon cancer and preventive implications. Cancer Biol. Ther. *8*, 1313–1317.

Croce, C.M. (2009). Causes and consequences of microRNA dysregulation in cancer. Nat. Rev. Genet. *10*, 704–714.

da Costa, L.T., He, T.C., Yu, J., Sparks, A.B., Morin, P.J., Polyak, K., Laken, S., Vogelstein, B., and Kinzler, K.W. (1999). CDX2 is mutated in a colorectal cancer with normal APC/beta-catenin signaling. Oncogene *18*, 5010–5014.

De Roock, W., De Vriendt, V., Normanno, N., Ciardiello, F., and Tejpar, S. (2011). KRAS, BRAF, PIK3CA, and PTEN mutations: implications for targeted therapies in metastatic colorectal cancer. Lancet Oncol. *12*, 594–603.

Dehm, S., Senger, M.A., and Bonham, K. (2001). SRC transcriptional activation in a subset of human colon cancer cell lines. FEBS Lett. *487*, 367–371.

Frattini, M., Signoroni, S., Pilotti, S., Bertario, L., Benvenuti, S., Zanon, C., Bardelli, A., and Pierotti, M.A. (2005). Phosphatase protein homologue to tensin expression and phosphatidylinositol-3 phosphate kinase mutations in colorectal cancer. Cancer Res. *65*, 11227.

Gaedcke, J., Grade, M., Camps, J., Søkilde, R., Kaczkowski, B., Schetter, A.J., Difilippantonio, M.J., Harris, C.C., Ghadimi, B.M., Møller, S., et al. (2012). The rectal cancer microRNAome—microRNA expression in rectal cancer and matched normal mucosa. Clin. Cancer Res. *18*, 4919–4930.

Ghafouri-Fard, S., Ousati Ashtiani, Z., Sabah Golian, B., Hasheminasab, S.M., and Modarressi, M.H. (2010). Expression of two testis-specific genes, SPATA19 and LEMD1, in prostate cancer. Arch. Med. Res. *41*, 195–200.

Grivennikov, S., Karin, E., Terzic, J., Mucida, D., Yu, G.Y., Vallabhapurapu, S., Scheller, J., Rose-John, S., Cheroutre, H., Eckmann, L., and Karin, M. (2009).

IL-6 and Stat3 are required for survival of intestinal epithelial cells and development of colitis-associated cancer. Cancer Cell *15*, 103–113.

Groden, J., Joslyn, G., Samowitz, W., Jones, D., Bhattacharyya, N., Spirio, L., Thliveris, A., Robertson, M., Egan, S., Meuth, M., et al. (1995). Response of colon cancer cell lines to the introduction of APC, a colon-specific tumor suppressor gene. Cancer Res. *55*, 1531–1539.

Guda, K., Giardina, C., Nambiar, P., Cui, H., and Rosenberg, D.W. (2001). Aberrant transforming growth factor-beta signaling in azoxymethane-induced mouse colon tumors. Mol. Carcinog. *31*, 204–213.

Han, M., Toli, J., and Abdellatif, M. (2011). MicroRNAs in the cardiovascular system. Curr. Opin. Cardiol. *26*, 181–189.

Hart, J.R., Liao, L., Ueno, L., Yates, J.R., 3rd, and Vogt, P.K. (2011). Protein expression profiles of C3H 10T1/2 murine fibroblasts and of isogenic cells transformed by the H1047R mutant of phosphoinositide 3-kinase (PI3K). Cell Cycle *10*, 971–976.

Hinoi, T., Akyol, A., Theisen, B.K., Ferguson, D.O., Greenson, J.K., Williams, B.O., Cho, K.R., and Fearon, E.R. (2007). Mouse model of colonic adenoma-carcinoma progression based on somatic Apc inactivation. Cancer Res. *67*, 9721–9730.

Hoogeboom, D., Essers, M.A., Polderman, P.E., Voets, E., Smits, L.M., and Burgering, B.M. (2008). Interaction of FOXO with beta-catenin inhibits beta-catenin/T cell factor activity. J. Biol. Chem. *283*, 9224–9230.

Ilyas, M., Tomlinson, I.P., Rowan, A., Pignatelli, M., and Bodmer, W.F. (1997). Beta-catenin mutations in cell lines established from human colorectal cancers. Proc. Natl. Acad. Sci. USA *94*, 10330–10334.

Kasinski, A.L., and Slack, F.J. (2011). Epigenetics and genetics. MicroRNAs en route to the clinic: progress in validating and targeting microRNAs for cancer therapy. Nat. Rev. Cancer *11*, 849–864.

Lee, G., Goretsky, T., Managlia, E., Dirisina, R., Singh, A.P., Brown, J.B., May, R., Yang, G.Y., Ragheb, J.W., Evers, B.M., et al. (2010). Phosphoinositide 3-kinase signaling mediates beta-catenin activation in intestinal epithelial stem and progenitor cells in colitis. Gastroenterology *139*, 869–881, e1–e9.

Leedham, S.J., Graham, T.A., Oukrif, D., McDonald, S.A., Rodriguez-Justo, M., Harrison, R.F., Shepherd, N.A., Novelli, M.R., Jankowski, J.A., and Wright, N.A. (2009). Clonality, founder mutations, and field cancerization in human ulcerative colitis-associated neoplasia. Gastroenterology *136*, 542–550, e6.

Lewis, B.P., Shih, I.H., Jones-Rhoades, M.W., Bartel, D.P., and Burge, C.B. (2003). Prediction of mammalian microRNA targets. Cell *115*, 787–798.

Mahon, P.C., Hirota, K., and Semenza, G.L. (2001). FIH-1: a novel protein that interacts with HIF-1alpha and VHL to mediate repression of HIF-1 transcriptional activity. Genes Dev. *15*, 2675–2686.

Marsh, V., Winton, D.J., Williams, G.T., Dubois, N., Trumpp, A., Sansom, O.J., and Clarke, A.R. (2008). Epithelial Pten is dispensable for intestinal homeostasis but suppresses adenoma development and progression after Apc mutation. Nat. Genet. *40*, 1436–1444.

Matsuyama, H., Suzuki, H.I., Nishimori, H., Noguchi, M., Yao, T., Komatsu, N., Mano, H., Sugimoto, K., and Miyazono, K. (2011). miR-135b mediates NPM-ALK-driven oncogenicity and renders IL-17-producing immunophenotype to anaplastic large cell lymphoma. Blood *118*, 6881–6892.

Morin, P.J., Vogelstein, B., and Kinzler, K.W. (1996). Apoptosis and APC in colorectal tumorigenesis. Proc. Natl. Acad. Sci. USA *93*, 7950–7954.

Moyer, M.P., Stauffer, J.S., Manzano, L.A., Tanzer, L.R., and Merriman, R.L. (1996). NCM460, a normal human colon mucosal epithelial cell line. In Vitro Cell Dev. Biol. Anim. *32*, 315–317.

Mukherji, S., Ebert, M.S., Zheng, G.X., Tsang, J.S., Sharp, P.A., and van Oudenaarden, A. (2011). MicroRNAs can generate thresholds in target gene expression. Nat. Genet. *43*, 854–859.

Nagel, R., le Sage, C., Diosdado, B., van der Waal, M., Oude Vrielink, J.A., Bolijn, A., Meijer, G.A., and Agami, R. (2008). Regulation of the adenomatous polyposis coli gene by the miR-135 family in colorectal cancer. Cancer Res. *68*, 5795–5802.

Necela, B.M., Carr, J.M., Asmann, Y.W., and Thompson, E.A. (2011). Differential expression of microRNAs in tumors from chronically inflamed or genetic (APC(Min/+)) models of colon cancer. PLoS ONE *6*, e18501.

Prahallad, A., Sun, C., Huang, S., Di Nicolantonio, F., Salazar, R., Zecchin, D., Beijersbergen, R.L., Bardelli, A., and Bernards, R. (2012). Unresponsiveness of colon cancer to BRAF(V600E) inhibition through feedback activation of EGFR. Nature *483*, 100–103.

Qian, J., Sarnaik, A.A., Bonney, T.M., Keirsey, J., Combs, K.A., Steigerwald, K., Acharya, S., Behbehani, G.K., Barton, M.C., Lowy, A.M., and Groden, J. (2008). The APC tumor suppressor inhibits DNA replication by directly binding to DNA via its carboxyl terminus. Gastroenterology *135*, 152–162.

Rehmsmeier, M., Steffen, P., Hochsmann, M., and Giegerich, R. (2004). Fast and effective prediction of microRNA/target duplexes. RNA *10*, 1507–1517.

Rojas, A., Padidam, M., Cress, D., and Grady, W.M. (2009). TGF-beta receptor levels regulate the specificity of signaling pathway activation and biological effects of TGF-beta. Biochim. Biophys. Acta *1793*, 1165–1173.

Samuels, Y., Diaz, L.A., Jr., Schmidt-Kittler, O., Cummins, J.M., Delong, L., Cheong, I., Rago, C., Huso, D.L., Lengauer, C., Kinzler, K.W., et al. (2005). Mutant PIK3CA promotes cell growth and invasion of human cancer cells. Cancer Cell *7*, 561–573.

Sansom, O.J., Reed, K.R., Hayes, A.J., Ireland, H., Brinkmann, H., Newton, I.P., Batlle, E., Simon-Assmann, P., Clevers, H., Nathke, I.S., et al. (2004). Loss of Apc in vivo immediately perturbs Wnt signaling, differentiation, and migration. Genes Dev. *18*, 1385–1390.

Sansom, O.J., Reed, K.R., van de Wetering, M., Muncan, V., Winton, D.J., Clevers, H., and Clarke, A.R. (2005). Cyclin D1 is not an immediate target of beta-catenin following Apc loss in the intestine. J. Biol. Chem. *280*, 28463–28467.

Sansom, O.J., Meniel, V.S., Muncan, V., Phesse, T.J., Wilkins, J.A., Reed, K.R., Vass, J.K., Athineos, D., Clevers, H., and Clarke, A.R. (2007). Myc deletion rescues Apc deficiency in the small intestine. Nature *446*, 676–679.

Serrels, A., Macpherson, I.R., Evans, T.R., Lee, F.Y., Clark, E.A., Sansom, O.J., Ashton, G.H., Frame, M.C., and Brunton, V.G. (2006). Identification of potential biomarkers for measuring inhibition of Src kinase activity in colon cancer cells following treatment with dasatinib. Mol. Cancer Ther. *5*, 3014–3022.

Shaulian, E. (2010). AP-1—The Jun proteins: Oncogenes or tumor suppressors in disguise? Cell. Signal. *22*, 894–899.

Sjöblom, T., Jones, S., Wood, L.D., Parsons, D.W., Lin, J., Barber, T.D., Mandelker, D., Leary, R.J., Ptak, J., Silliman, N., et al. (2006). The consensus coding sequences of human breast and colorectal cancers. Science *314*, 268–274.

Valeri, N., Croce, C.M., and Fabbri, M. (2009). Pathogenetic and clinical relevance of microRNAs in colorectal cancer. Cancer Genomics Proteomics *6*, 195–204.

Valeri, N., Gasparini, P., Fabbri, M., Braconi, C., Veronese, A., Lovat, F., Adair, B., Vannini, I., Fanini, F., Bottoni, A., et al. (2010). Modulation of mismatch repair and genomic stability by miR-155. Proc. Natl. Acad. Sci. USA *107*, 6982–6987.

Waugh, D.J., and Wilson, C. (2008). The interleukin-8 pathway in cancer. Clin. Cancer Res. *14*, 6735–6741.

Xu, X.L., Yu, J., Zhang, H.Y., Sun, M.H., Gu, J., Du, X., Shi, D.R., Wang, P., Yang, Z.H., and Zhu, J.D. (2004). Methylation profile of the promoter CpG islands of 31 genes that may contribute to colorectal carcinogenesis. World J. Gastroenterol. *10*, 3441–3454.

Yeatman, T.J. (2004). A renaissance for SRC. Nat. Rev. Cancer *4*, 470–480.

Yoon, J., Koo, K.H., and Choi, K.Y. (2011). MEK1/2 inhibitors AS703026 and AZD6244 may be potential therapies for KRAS mutated colorectal cancer that is resistant to EGFR monoclonal antibody therapy. Cancer Res. *71*, 445–453.

Yuki, D., Lin, Y.M., Fujii, Y., Nakamura, Y., and Furukawa, Y. (2004). Isolation of LEM domain-containing 1, a novel testis-specific gene expressed in colorectal cancers. Oncol. Rep. *12*, 275–280.